Synthesis and characterization of the multi-photon absorption and excited-state properties of a neat liquid 4-propyl 4′-butyl diphenyl acetylene†

Iam Choon Khoo,*[a] Scott Webster,[b] Shoichi Kubo,[c] W. Justin Youngblood,[d] Justin D. Liou,[a] Thomas E. Mallouk,[e] Ping Lin,[f] David J. Hagan[b] and Eric W. Van Stryland[b]

The synthesis, characterization, and quantitative electronic structure modeling of multi-photon absorption properties of a neat liquid L34 (4-propyl 4′-butyl diphenyl acetylene) are reported. The liquid is (linearly) transparent in the visible spectrum, but possesses large two-photon absorption (2PA) and 2PA-induced singlet and triplet excited-state absorption as measured by the Z-scan technique and non-linear transmission measurements using both picosecond and nanosecond pulses. The most dominant contributions to the intensity-dependent non-linear absorption come from the 2PA-induced triplet excited states in the nanosecond time regime. We also present transient absorption spectra of the liquid obtained by nanosecond laser-flash photolysis and compare these results with electronic structure calculations. The energy of the absorption bands, both singlet and triplet are in reasonable agreement with calculations performed with Gaussian 03. The experimentally measured spectra and theoretical electronic structure modeling provide information about the energy levels of the excited states of this liquid, including 2PA and 2PA-induced process that is responsible for its non-linear optical properties.

Introduction

Pulsed and continuous-wave lasers are now extensively used in various settings. Direct intentional or accidental exposure to such intense radiation could lead to 'flash blindness' or severe permanent damage to the sensors, e.g. the eye.[1] Although fixed-wavelength filters offer effective protection from lasers of known wavelengths, they are ineffective against agile frequency lasers, the wavelengths of which can be anywhere in the UV to infrared. Next generation organic material based electro-optical devices, e.g. tunable filters where the transmission window can be electronically tuned away from the incident laser wavelength, and various other liquid crystalline materials and devices,[2–5] are effective against continuous-wave (CW) or long-pulse (microseconds to 10s of nanoseconds) lasers but cannot respond fast enough to mitigate very short laser pulses in the nano- and sub-nano-second time scales. For applications in the latter time scales, non-linear absorbing materials capable of very fast all-optical switching operations have been actively investigated.[2–16]

Examples are materials that possess multi-photon absorption properties such as reverse saturable absorption (RSA),[6–9] two-photon absorption (2PA) and excited state absorption (ESA)[10–20] and non-linear scattering properties.[21] These materials allow maximal transmission at low input light intensity level, but become increasingly 'opaque' via a variety of non-linear optical processes as the incident light intensity increases, in such a manner that the energy of the transmitted laser pulse is clamped below the damage threshold of the sensor. In general, RSA materials have low switching threshold, but they are (linearly) absorptive, and could be easily 'bleached' by high intensity laser. Although two-photon absorbers are more desirable because they are linearly transparent, efficient 2PA materials that activate non-linear absorption at low threshold are also susceptible to bleaching by high intensity lasers. To extend the operational dynamic range, materials that possess simultaneously large two-photon and excited-state absorption cross-sections, c.f. Fig. 1, have become the central focus of many material development efforts.

Most 2PA materials are in powdery solid form; as a result of their low solubility and/or intermolecular interactions, the transmittance changes induced by non-linear absorption in solutions of 2PA are small. One technique often employed is the engineering of chromophores with large dendrimers and peripheral substitutions to allow for increased concentrations while suppressing aggregation and unwanted intermolecular interactions. Although these techniques can increase solubility, and thereby non-linear absorption, maximum concentrations of 2PA chromophores are typically small, on the order of 10^{-3} to 10^{-2} M in solution. Neat liquids of 2PA chromophores, such as L34[16–19] or liquid crystals in their isotropic phase,[20] are attractive for their ability to maintain their linear and NLO properties at 100% concentration even when their 2PA cross sections are

[a]Department of Electrical Engineering, The Pennsylvania State University, University Park, PA, 16802, USA. E-mail: ick1@psu.edu
[b]CREOL, The College of Optics and Photonics, University of Central Florida, Orlando, FL, 32826, USA
[c]Institute of Multidisciplinary Research for Advanced Materials, Tohoku University, 2-1-1 Katahira, Aoba-ku, Sendai, 980-8577, Japan
[d]Department of Chemistry, University of North Texas, 1155 Union Circle, # 305070, Denton, TX, 76203, USA
[e]Department of Chemistry, The Pennsylvania State University, University Park, PA, 16802, USA
[f]Materials Research Institute, The Pennsylvania State University, University Park, PA, 16802, USA
† This paper is part of a Journal of Materials Chemistry theme issue on organic non-linear optics. Guest editor: Seth Marder.
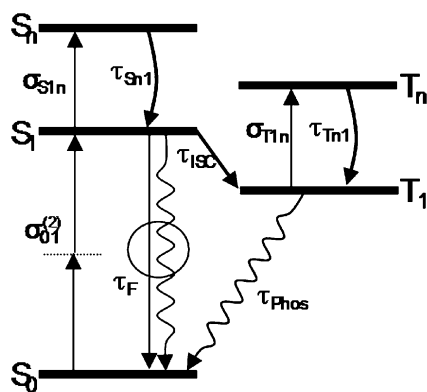
Fig. 1 Energy level schematic for 2PA ($\sigma_{01}^{(2)}$) with 2PA-induced ESA from singlet (σ_{S1n}) and triplet (σ_{T1n}) excited states.

relatively smaller. Designing new neat liquids, with additional non-linear absorption mechanisms, will increase their effective 2PA cross sections and allow for applications requiring large non-linear absorptions.

Previously[18,19] we have reported a neat organic liquid 4-propyl 4′-butyl diphenyl acetylene (L34) that exhibits two-photon mediated excited state absorption (2P-ESA). L34 is a neat liquid over a wide temperature range, including room temperature, and has a high transmittance in the visible wavelength region. In order to further understand these 2P-ESA properties, it is important to characterize its manifold of electronic excited states. The lowest energy triplet state (T_1) is one of the most important states because it can be populated by intersystem crossing from excited singlet states, typically the first excited state (S_1). Intersystem crossing can affect non-linear absorption strongly by opening additional channels of triplet-triplet excitation and non-radiative decay to the ground state (S_o).

Experimental

Synthesis and chemical characterization of L34 (4-propyl 4′-butyl diphenyl acetylene)

L34 was synthesized following the route depicted in Fig. 2. Compound **1**, 4-(4-butylphenyl)-2-methylbut-3-yn-2-ol, was synthesized as described in previous reports.[22–25] A Schlenk

reaction flask was charged with 1-bromo-4-butylbenzene (25.0 g, 117 mmol), PdCl$_2$(PPh$_3$)$_2$ (4.11 g, 5.86 mmol), CuI (1.12 g, 5.88 mmol), and PPh$_3$ (3.07 g, 11.7 mmol). The flask was evacuated and refilled with nitrogen three times. Then a nitrogen-sparged sample of 2-methyl-3-butyn-2-ol (14.8 g, 176 mmol) in triethylamine (TEA) (150 mL) was transferred to the reaction flask. The mixture was refluxed overnight with stirring. Upon cooling to room temperature, the crude reaction mixture was diluted with ethyl acetate (EtOAc) and washed with water, followed by additional washings with saturated aqueous NH$_4$Cl, water, and brine. The organic layer was separated and dried over MgSO$_4$, filtered, and concentrated. The residue was chromatographed (SiO$_2$, hexanes/EtOAc 6:1) to obtain a colorless oil product (21.7 g, 86%). The compound was identified by ^{1}H NMR and carried forward to the next reaction without further characterization.

To obtain 1-butyl-4-ethynylbenzene (**2**), a finely ground sample of NaOH (44 g, 1.1 mol) was added to a solution of **1** (11.9 g, 55.0 mmol) in toluene (250 mL). The mixture was refluxed with stirring for 10 h. The reaction mixture was filtered, and then washed with water, followed by brine treatment. The toluene layer was separated and dried over MgSO$_4$, filtered, and concentrated. The residue was chromatographed (SiO$_2$, hexanes) and fractions containing the desired product were distilled at reduced pressure to obtain **2** as a colorless oil (7.36 g, 85%). To obtain the final product, 4-propyl-4′-butyl diphenyl acetylene (L34), a Schlenk reaction flask was charged with **2** (7.35 g, 46.4 mmol), PdCl$_2$(PPh$_3$)$_2$ (1.50 g, 2.14 mmol), CuI (406 mg, 2.13 mmol), and PPh$_3$ (1.11 g, 4.23 mmol). The flask was evacuated and refilled with nitrogen gas three times. A nitrogen-sparged sample of 1-bromo-4-propylbenzene (8.4 g, 42.2 mmol) in TEA (150 mL) was transferred to the reaction flask. The mixture was refluxed overnight with stirring. Upon cooling to room temperature, the crude reaction mixture was diluted with EtOAc and washed with water, followed by additional washings with saturated aqueous NH$_4$Cl, water, and brine. The organic layer was separated and dried over MgSO$_4$, filtered, and concentrated. The residue was chromatographed (SiO$_2$, hexanes) and fractions containing the desired product were subjected to bulb-to-bulb distillation to obtain L34 as a colorless oil (7.40 g, 63%). GC-MS analysis indicated that the masses of the impurities (∼4%) contain the Glaser-coupled byproduct L44 (4,4′-dibutyldiphenylbutadiyne), a longer-central-chain
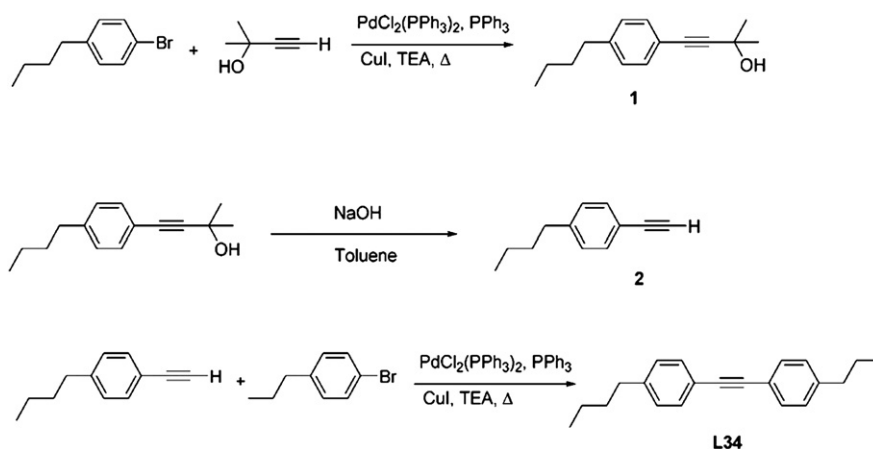

Fig. 2 Synthetic scheme of L34.

L34 (4-propyl 4'-butyl diphenyl acetylene)

Mol. Formula = $C_{21}H_{24}$
Mol. Weight = 276.41526

L44 (4,4'-dibutyldiphenylbutadiyne)

Mol. Formula = $C_{24}H_{26}$
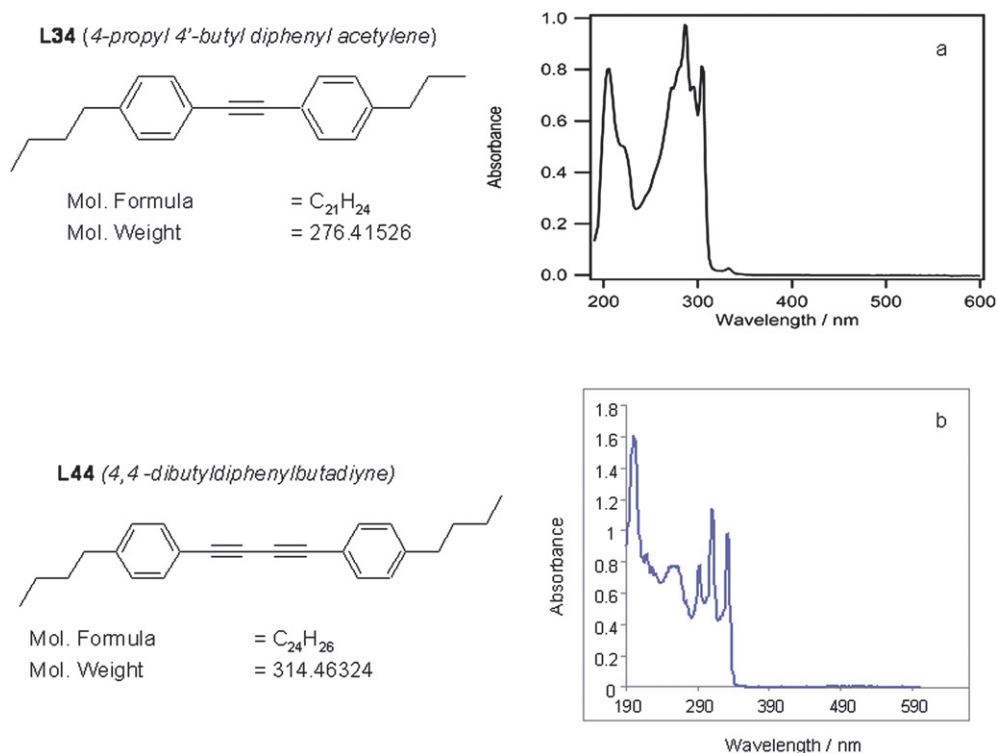Mol. Weight = 314.46324

Fig. 3 Molecular structures of L34 (a) and L44 (b) and their (linear) absorption spectra.

derivative of L34, cf. Fig. 3. L44 is a known organic solid compound. Its synthesis and liquid-crystalline properties were first reported by Grant.[26] In order to understand the nature of L44, and also to corroborate the quantum calculations and excited-state transient studies in the sections to follow, we have recently performed a separate synthesis effort of L44 and obtained its spectrum.

Fig. 3(a) shows a UV-visible absorption spectrum of L34 diluted in hexane. The liquid is transparent in the visible regime and begins to absorb at wavelengths shorter than ~300 nm. The absorption spectrum of L34 is similar to those of diphenylacetylene in solutions of glycerol and cyclohexane[23,27] except for some absorption peaks located near 310nm and 325 nm. These peaks are attributed to the presence of L44, the absorption spectrum of which is shown in Fig. 3(b). As our ESA experiments and electronic structure calculations in the following section will show, the longer conjugated central linker of L44 corresponds to lower excitation energies (longer wavelength); it also exhibits strong excited triplet state absorption.

Non-linear optical characterization

Non-linear optical investigations of L34 include a broad range of measurements facilitating a detailed study of lifetime dynamics, 2PA, and 2PA-induced ESA into both singlet and triplet states with self-consistent results across the measured laser pulse widths. The picosecond laser system consists of a 10 Hz mode-locked Nd:YAG laser (EKSPLA, model PL2143) and is externally frequency doubled to produce 532 nm with a pulse width of ~23 ps (FWHM), measured by second-harmonic autocorrelation. The nanosecond laser system is an externally frequency doubled 10 Hz, seeded Nd:YAG laser (Continuum, Powerlight

9010) with a pulse width of ~6 ns (FWHM) measured by a fast silicon detector and digital storage oscilloscope (Tektronix, TDS680C, 1GHz/5Gs) at 532 nm. All measurements were performed with neat-liquid samples in cell thicknesses dependent on the measurement techniques and geometries used. Focal spot sizes used for Z-scan and non-linear transmittance measurements were determined by measuring and modeling the non-linear refraction of carbon disulfide using the closed aperture Z-scan technique detailed in ref. 12 and 28. This method serves as a calibration for focused spot sizes and also as an irradiance calibration to double check the independently measured energy and temporal width of the laser pulse. Fluorescence lifetime measurements were obtained by a time-correlated single photon counting system (PicoQuant, PicoHarp300) with a time resolution of ~80 ps using a linear polarized frequency doubled femtosecond excitation at 390 nm and oriented at the magic angle (54.7 deg).

Laser-flash photolysis was performed using excitations of both third (355 nm) and fourth (266 nm) harmonics of a nanosecond Nd:YAG laser. Measurements were performed in quartz optical cells pumped by the Nd:YAG harmonics while changes in transmittance, probed with a Xe lamp, were monitored using a monochromator equipped with a photomultiplier tube detector. Measurements were averaged twenty times with a pump pulse repetition rate of 0.25 Hz at each wavelength.

Quantum chemical calculations

Quantum mechanical ab-initio calculations of the excited-state properties were computed using Gaussian 03[29] for several model main-chain molecules with various end/side groups. The ground and excited states of these molecules were investigated using the SAC (symmetry-adapted cluster)/SAC-CI (configuration

interaction) singles and doubles (SD)-R method as well as time-dependent density functional theory (TD-DFT).[30–32]

Results and discussion

Two-photon absorption and two-photon-induced excited state absorption

In order to understand and model the non-linear absorption processes, the population dynamics must be understood. For both picosecond and nanosecond measurements the non-linear absorption was modeled with the propagation and rate equations for 2PA-induced ESA as described by:

$$\frac{dI}{dz} = -\frac{\sigma_{01}^{(2)} N_{S0} I^2}{\hbar\omega} - \sigma_{S1n} N_{S1} I - \sigma_{T1n} N_{T1} I$$

$$\frac{dN_{S0}}{dt} = -\frac{\sigma_{01}^{(2)} N_{S0} I^2}{2(\hbar\omega)^2} + \frac{N_{S1}}{\tau_F} + \frac{N_{T1}}{\tau_{Phos}}$$

$$\frac{dN_{S1}}{dt} = \frac{\sigma_{01}^{(2)} N_0 I^2}{2(\hbar\omega)^2} - \frac{N_{S1}}{\tau_F} - \frac{\sigma_{S1n} N_{S1} I}{\hbar\omega} + \frac{N_{Sn}}{\tau_{Sn1}} - \frac{N_{S1}}{\tau_{ISC}} \quad (1)$$

$$\frac{dN_{Sn}}{dt} = \frac{\sigma_{S1n} N_{S1} I}{\hbar\omega} - \frac{N_{Sn}}{\tau_{n1}}$$

$$\frac{dN_{T1}}{dt} = -\frac{\sigma_{T1n} N_{T1} I}{\hbar\omega} + \frac{N_{Tn}}{\tau_{Tn1}} + \frac{N_{S1}}{\tau_{ISC}} - \frac{N_{T1}}{\tau_{Phos}}$$

$$\frac{dN_{Tn}}{dt} = \frac{\sigma_{T1n} N_{T1} I}{\hbar\omega} - \frac{N_{Tn}}{\tau_{Tn1}}$$

where N_{S0}, N_{S1}, N_{Sn}, N_{T1}, and N_{Tn} are the populations of each level ($N_{total} = N_{S0} + N_{S1} + N_{Sn} + N_{T1} + N_{Tn}$); $\sigma_{01}^{(2)}$, σ_{S1n}, and σ_{T1n} are the two-photon, singlet excited, and triplet ESA cross-sections, respectively. The fluorescence lifetime, τ_F, of L34 was experimentally determined to be $\tau_F = 2.1 \pm 0.2$ ns. The highest singlet, S_n, and triplet, T_n, excited states were assumed not to be populated since the lifetimes τ_{Sn1} and τ_{Tn1} are ultrafast compared to the pulse widths used in these experiments, and therefore can also be neglected, simplifying the rate equations in Eq. 1. All of the modeling in this section assumes that the recovery from the triplet to the ground singlet state is slow and can be neglected,

i.e., that the phosphorescence lifetime, τ_{Phos}, is much longer than tens of nanoseconds as described by the nanosecond laser-flash photolysis measurements in the following section.

Shown in Fig. 4(a) are the results of the picosecond Z-scan measurements at 532 nm modeled by Eq. 1. for determining the 2PA coefficient and 2PA-induced singlet ESA cross-section. For input energies ranging from 45nJ to 1.6μJ (a total transmittance change of ~60%) the 2PA coefficient β was determined to be 0.85 ± 0.15 cm/GW corresponding to a 2PA cross section $\sigma_{01}^{(2)}$ of ~18 ± 4 GM and a singlet ESA cross-section of $\sigma_{S1n} = 7.2 \pm 1.2 \times 10^{-18}$ cm² at 532 nm, using a neat liquid molecular density of $N_o = 1.588 \times 10^{21}$/cm³. The upper singlet excited-state lifetime, τ_{Sn1}, is determined to be ultrafast as compared to the picosecond pulsewidth. Fig. 4(b) shows the nanosecond non-linear transmittance results also modeled by Eq. 1. which includes 2PA and 2PA-induced ESA from both singlet and triplet states. Laser-induced breakdown is observed for input energies greater than 100 μJ as evidenced by the sharp drop in transmittance. For nanosecond pulse widths, there is sufficient time to populate the triplet state, T_1, therefore this population needs to be included. To fully determine the singlet–triplet dynamics, both fluorescence lifetime and a long pulse-width measurement (nanosecond Z-scan or non-linear transmittance) must be performed in order to decouple the triplet intersystem crossing rate and yield. Using the fluorescence lifetime measurement and the picosecond Z-scan results of 2PA and 2PA-induced singlet ESA cross-sections as initial fitting parameters, the nanosecond non-linear transmittance data was fit to obtain $\alpha_2 = 0.75 \pm 0.15$ cm/GW, $\sigma_{S1n} = 6 \pm 1.2 \times 10^{-18}$ cm², $\sigma_{T1n} = 1.2 \pm 0.3 \times 10^{-16}$ cm², and $\tau_{ISC} = 17 \pm 5$ ns. These values are found to be in excellent agreement with the corresponding picosecond Z-scan measurements. The triplet yield Φ_T (calculated from $\Phi_T = \tau_F/(\tau_F + \tau_{ISC})$) is determined to be ~10 ± 2%.

As previously alluded to, a large 2PA cross section alone may not necessarily lead to large non-linear absorption changes needed for applications. A material that combines the ability for large concentrations (neat liquids being the most ideal ones) with
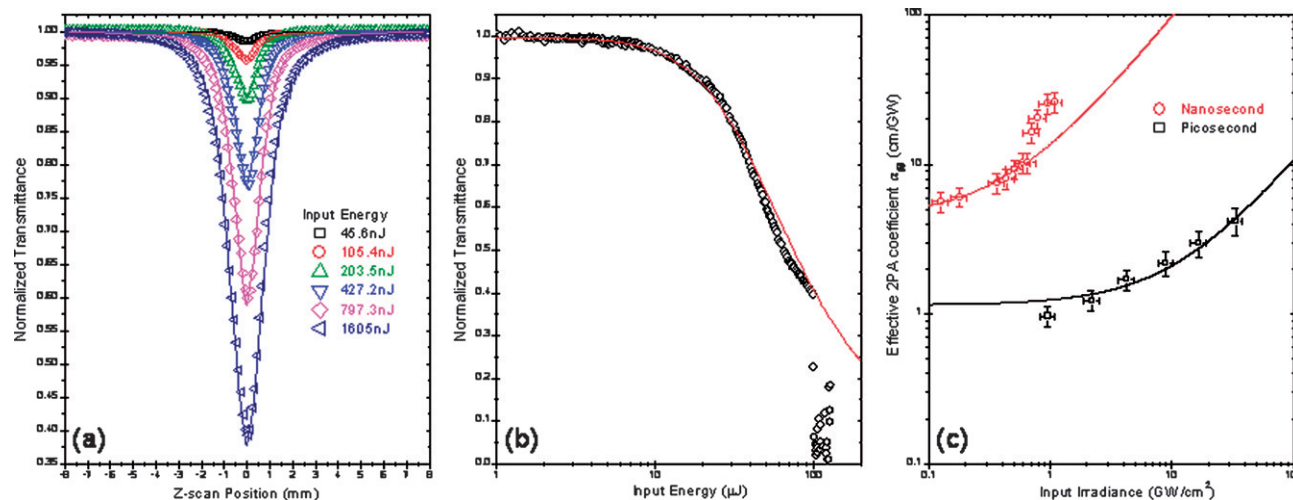

Fig. 4 (a) Picosecond Z-scan results at 532 nm. (b) Nanosecond non-linear transmittance results at 532 nm. (c) Effective 2PA coefficients as a function of irradiance for both nanosecond (red circles) and picosecond (black squares) pulse widths. Note: solid lines are linear regressions that appear non-linear on the logarithmic scales.

several non-linear absorption mechanisms is desired. Fig. 4(c) shows the effective 2PA coefficient α_2 versus input irradiance for both picosecond and nanosecond pulse widths. An effective 2PA coefficient α_2 is the result of modeling the total non-linear absorption as if it were only due to 2PA, *i.e.*, pure Im $[\chi^{(3)}]$. The 2PA coefficient, β, is independent of irradiance while the effective 2PA coefficient includes additional non-linear absorption mechanisms that cause an increasing dependence when plotted versus irradiance. An estimate for the intrinsic 2PA coefficient β can be obtained by extrapolating the linear fit of α_2 to zero input irradiance when the contributions from other non-linear mechanisms are small. Clearly, the nanosecond data show larger values due to the combined non-linearities of 2PA and 2PA-induced ESA from both singlet and triplet absorptions whereas the picosecond data only include contributions from 2PA and 2PA-induced singlet excited-state absorption. Linear extrapolation to zero input irradiance works fairly well for the picosecond results but not for the nanosecond results since its non-linear absorption is dominated mostly by ESA from both singlet and triplet states. From the modeled data in Fig. 4(a) and (b), the 2PA absorption coefficient in L34 is determined to be $\beta = 0.8 \pm 0.2$ cm/GW while the nanosecond data in Fig. 4(c) show effective 2PA coefficients α_2 from 5 to 30 cm/GW corresponding to an order of magnitude increase due to these combined non-linearities.

Transient excited-state absorption and quantum mechanical calculations

In view of the critical role played by triplet ESA that underlie the superb all-optical switching performance of L34,[17–19] we have performed quantum mechanical electronic structure calculations of the excited-state energies and dipole transition strengths and present the findings here with corroborating transient ESA spectra obtained by nanosecond laser-flash photolysis.

The excited-state properties were computed using Gaussian 03[29] for several model main-chain molecules including DPY1 (diphenyl acetylene) and DPY2 (1,4-diphenylbutadiyne) with various end/side groups, *cf.* Fig. 5. Note that in this notation, L34 becomes DPY1-L34 and L44 becomes DPY2-L44. The 1 and 2 after "DPY" denotes the number of central linkage groups. The calculated molecular orbitals (MO) for DPY1 are composed primarily of π-type orbitals, and the highest occupied MOs (HOMO) and lowest unoccupied MOs (LUMO) are similar to those calculated in an earlier study.[33] The ground and excited states of these molecules were investigated using the SAC/SAC-CI (SD)-R method as well as TD-DFT. Information about the singlet ground and excited states obtained using TD-DFT is presented in Tables 1 and 2, respectively. The calculated singlet and triplet excitation energies in eV, and their corresponding
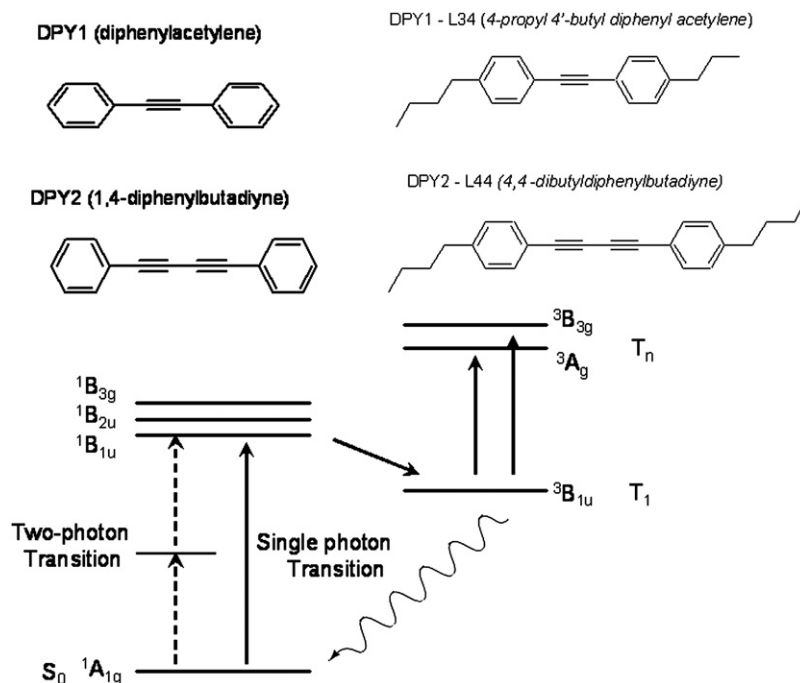

Fig. 5 Schematic of the main chain molecules DPY1 and DPY2 and some singlet–triplet energy levels used in the computation.

Table 1 Energies associated with singlet excitation for DPY1 (diphenyl acetylene), DPY1-L34 (4-propyl 4′-butyl diphenyl acetylene), DPY2 (1,4-diphenylbutadiyne), DPY2-L44 (4,4′-butyl 1,4-diphenylbutadiyne), DPY2-L33 (4,4′-propyl 1,4-diphenylbutadiyne) and DPY2-L34 (4,4′-butyl 1,4-diphenylbutadiyne)

	DPY1	DPY1-L34	DPY2	DPY2-L44	DPY2-L33	DPY2-L34
$S_0(^1A_g)$–$S_3(^1B_{1u})$/eV	4.0948	3.9779	3.6009	3.5289	3.5319	3.5302
$S_0(^1A_g)$–$S_3(^1B_1)$/nm	302.78	311.69	344.31	351.34	351.04	351.21
Osc. strength	0.9482	1.3049	0.9456	1.2897	1.2610	1.2744
Expt./eV (gas, ref. 35)	4.37					
Expt./eV (sol., ref. 34)	4.073		3.712			

Table 2 Energies associated with triplet excitation: theoretical results from TD-DFT calculations. T_1–T_n represents the strongest excitation, T_1–T_n' and T_1–T_n'' represent the weaker excitations

	DPY1	DPY1-L34	DPY2	DPY2-L44	DPY2-L33	DPY2-L34
$T_1(^3B_{1u})$–$T_n(^3A_g)$/eV	2.9865	2.8037	2.7076	2.5710	2.5781	2.5745
T_1–T_n/nm	415.15	442.22	457.92	482.24	480.91	481.58
T_1–T_n/Osc.strength	1.2311	1.3571	1.4324	1.8290	1.7952	1.8101
T_1–T_n'/eV		2.5997		2.8540	2.8609	2.8577
T_1–T_n'/nm		476.92		434.43	433.38	433.85
T_1–T_n'/Osc. strength		0.1127		0.0238	0.0213	0.0225
T_1–T_n''/eV		2.7712				
T_1–T_n''/nm		447.40				
T_1–T_n''/Osc. strength		0.0174				
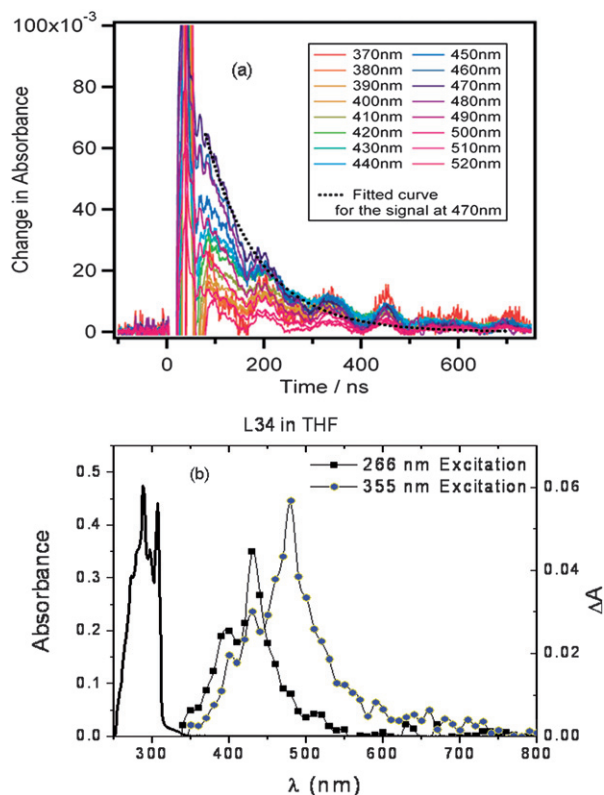
Fig. 6 (a) Time evolution of the changes in absorbance at various wavelengths following a ~7 ns laser flash at 355 nm. (b) Transient excited-state absorption spectra obtained with 266 nm (squares) and 355 nm (circles) laser excitation; the solid line is the ground-state linear absorption spectrum for reference purposes.

wavelengths, are in good agreement with previously reported experimental observations.[34–36] For example, SAC-CI calculations of the DPY1 molecule using the 6-311G(d,p) basis set gave an energy of 4.54 eV for the $S_0(^1A_g)$–$S_3(^1B_{1u})$ excitation, in reasonable agreement with experimental values of 4.07 eV [ref. 34, measurement in methylcyclohexane solution] and 4.37 eV (35,248 cm^{-1}) [ref. 35, measurement in the gaseous state]. The excitation energies of the $S_0(^1A_g)$–$S_1(^1B_{2u})$ and $S_0(^1A_g)$–$S_2(^1B_{3g})$ transitions were calculated to be 4.797 and 4.804 eV, respectively, while the corresponding experimental values are 4.346 eV (35 051 cm^{-1})[36] and 4.334 eV (34 960 cm^{-1}).[35] The discrepancy is in part due to the differences between vertical and adiabatic transitions.

Of particular interest to the present studies are the excited-state $T_1(^3B_{1u}) \rightarrow T_n(^3A_g)$ transitions. As listed in Table 2, the transition energies (in eV) and wavelengths for DPY1-L34 are 2.80 eV and 443 nm, while for DPY2-L33, -L34 and -L44, they are ~2.57 eV and 482 nm, respectively. It is to be noted that these excited-state transition energies decrease with longer central linkage but do not vary appreciably as we alter the side groups. These calculations are corroborated by transient absorption spectroscopy. From the linear absorption spectrum in Fig. 3, as well as the electronic structure calculations in the preceding section, the 266 nm excitation will access the singlet excited states of L34 (DPY1-L34) whereas the longer-wavelength 355 nm excitation will access the triplet excited states of the by-product L44 (DPY2-L44). Fig. 6(a) shows a typical transient absorption induced by laser-flash photolysis. Very similar decay curves were observed at all wavelengths between 370 and 520 nm after 355 nm excitation. The trace collected at 470 nm was used for analysis. It was fit to a single exponential function (dotted line in Fig. 6(a)), with the lifetime of 110 ns ± 2 ns. From these traces, a transient absorption spectrum was compiled 100 ns after excitation. The results (355 nm) along with a separate study pumped with 266 nm excitation are plotted in Fig. 6(b). In the case of 266 nm excitation, a broad absorption band that peaks at 440 nm was obtained and is attributed to L34 (DPY1-L34), whereas the 355 nm excitation yields a broad absorption band that peaks at 480 nm, attributed to L44 (DPY2-L44).

Conclusions

The 2PA-induced ESA of the neat liquid, L34, containing some of its longer main-chain derivatives have been investigated both experimentally, using non-linear transmission techniques and transient absorption spectroscopy, and theoretically using quantum mechanical ab-initio calculations. Measurements made with both picosecond and nanosecond pulse widths to quantify 2PA and 2PA-induced ESA from both singlet and triplet excited states are in excellent agreement. Modeling of these data, using a five-level model, resulted in the following parameters: 2PA coefficient, $\beta = 0.8 \pm 0.2$ cm/GW; singlet ESA cross section, $\sigma_{S1n} = 6.6 \pm 1.5 \times 10^{-18}$ cm²; triplet ESA cross section, $\sigma_{T1n} = 1.2 \pm 0.3 \times 10^{-16}$ cm²; singlet–triplet intersystem crossing lifetime, $\tau_{ISC} = 17 \pm 5$ ns; and triplet yield, 10 ± 2%. The quantum mechanical calculations for the triplet excited-state transition are in good agreement with the experimentally obtained ESA spectra. These results are important for

understanding the excited-state structures of L34 and provide insights into designing new efficient non-linear absorbers at longer wavelengths.

References

1 ANSI Standard Z136.1. *American National Standard for the Safe Use of Lasers*. American National Standards Institute, Inc., New York 2000.
2 A. Urbas, J. Klosterman, V. Tondiglia, L. Natarajan, R. Sutherland, S. Tsutsumi, T. Ikeda and T. Bunning, *Adv. Mat.*, 2004, **16**, 1453–1456.
3 I. C. Khoo, *Phys. Report*, 2009, **471**, 221–267.
4 I. C. Khoo, J. H. Park and J. D. Liou, *Appl. Phys. Letts.*, 2007, **90**, Art. # 151107.
5 I. C. Khoo, J. H. Park and J. D. Liou, *J. Opt. Soc. Am.*, 2008, **B25**, 1931–1937.
6 J. W. Perry, K. Mansour, S. R. Marder, K. J. Perry, D. Alvarez and I. Choong, *Opt. Letts.*, 1994, **19**, 625–627.
7 C. W. Spangler, *J. Mater. Chem.*, 1999, **9**, 2013–2020.
8 J. S. Shirk, G. S. Pong, F. J. Bartoli and A. W. Snow, *Appl. Phys. Letts.*, 1993, **63**, 1880–1882.
9 R. L. Sutherland, M. C. Brant, D. M. Brandelik, P. A. Fleitz, D. G. McLean and T. Pottenger, *Optics Letters*, 1993, **18**, 858–860.
10 J. Barroso, A. Costela, I. Garcia-Moreno and J. L. Saiz, *Journal of Physical Chemistry A*, 1998, **102**, 2527–2532.
11 G. S. He, L. S. Tan, Q. Zheng and P. N. Prasad, *Chem. Rev.*, 2008, **108**, 1245–1330.
12 M. Sheik-Bahae, A. A. Said, T. H. Wei, D. J. Hagan and E. W. Van Stryland, *IEEE J. Quant. Electron.*, 1990, **26**, 760–769.
13 J. E. Ehrlich, X. L. Wu, I. Y. S. Lee, Z. Y. Hu, H. Rockel, S. R. Marder and J. W. Perry, *Optics Letters*, 1997, **22**, 1843–1845.
14 I. C. Khoo, M. V. Wood, B. D. Guenther, M.-Yi Shih, P. H. Chen, Z. Chen and X. Zhang, *Optics Express*, 1998, **2**(12), 471–482.
15 I. C. Khoo, P. H. Chen, M. V. Wood and M.-Y. Shih, *Chemical Physics*, 1999, **245**, 517–531.
16 I. C. Khoo, M. V. Wood, B. D. Guenther, M.-Y. Shih and P. H. Chen, *J. Opt. Soc. Am. B*, 1998, **15**, 1533–1540.
17 I. C. Khoo, A. Diaz, M. V. Wood and P. H. Chen, *IEEE Journal on Selected Topics in Quantum Electronics*, 2001, **7**, 760–768.
18 I. C. Khoo, A. Diaz and J. Ding, *J. Opt. Soc. Am. B*, 2004, **21**, 1234–1240.
19 I. C. Khoo, *IEEE J. Selected Topics in Quantum Electronics JSTQE*, 2008, **14**(3), 946–951.
20 G. S. He, T.-C. Lin, P. N. Prasad, C.-C. Cho and L.-J. Yu, *Appl. Phys. Letts.*, 2003, **82**, 4717–4719.
21 K. Mansour, M. J. Soileau and E. W. VanStryland, *J. Opt. Soc. Am.*, 1992, **B9**, 1100–1109.
22 J.-H. B. Meng, L. D. Dalton and S.-T. Wu, *Mol. Cryst. Liq. Cryst.*, 1994, **250**, 303–314.
23 N. Miyaura and A. Suzuki, *Chem. Rev.*, 1995, **95**, 2457–2483.
24 C. Sekine, K. Iwakura, N. Konya, M. Minai and K. Fujisawa, *Liq. Cryst.*, 2001, **28**, 1375–1387.
25 Y. Fujita, Y. Misumi, M. Tabata and T. Masuda, *J. Polym. Sci. Pol. Chem.*, 1998, **36**, 3157–3163.
26 B. Grant, *Mol. Cryst. Liq. Cryst.*, 1978, **vol. 48**, 175–182.
27 Y. Hirata, T. Okada and T. Nomoto, *Chem. Phys. Lett.*, 1998, **293**, 371–377.
28 M. Sheik-Bahae, A. A. Said and E. W. Van Stryland, *Opt. Lett.*, 1989, **14**, 955–957.
29 M. J. Frisch *et al.*, *Gaussian 03*; Gaussian, Inc.: Wallingford CT, (2004).
30 H. Nakatsuji, *Chem. Phys. Lett.*, 1979, **67**, 329–333.
31 H. Nakatsuji, *Chem. Phys. Lett.*, 1979, **67**, 334–342.
32 N. Nakatsuji, *Chem. Phys. Lett.*, 1978, **59**, 362–364.
33 Y. Amatatsu and M. Hosokawa, *J. Phys. Chem. A*, 2004, **108**, 10238–10244.
34 Y. Nagano, T. Ikoma, K. Akiyama and S. Tero-Kubota, *JACS*, 2003, **125**, 14103–14112.
35 K. Okuyama, M. C. R. Cockett and K. Kimura, *J. Chem. Phys.*, 1992, **97**, 1649–1654.
36 K. Okuyama, T. Hasegawa, M. Ito and N. Mikami, *J. Phys. Chem.*, 1984, **88**, 1711–1716.

This journal is © The Royal Society of Chemistry 2009

J. Mater. Chem., 2009, **19**, 7525–7531 | 7531